CHAPTER 8

Approaching Control Based on Mobile Tether Attachment Points

The orbit control during the approaching target phase is one of the key missions for the TSR and has been studied by many researchers. A new method is proposed by Pradeep [1] to determine the tension control law, which is designed based on theorems in analytical mechanics. Nakamura discussed the collaborative control of the tension (controlled by the service satellite) and thruster (controlled by tethered robot) in approaching the target of the tethered retriever but the attitude is not considered [2]. A boundary control was proposed for station keeping of a tethered satellite system in the literature [3], but the proposed boundary controller does not constrain the tension in the tether to be positive. Modi et al. [4] investigated an off-set control strategy that uses a manipulator mounted on the platform to regulate the tether swing. The corresponding state feedback controller is designed using a graph theoretic approach and the tethered system is successfully regulated by the controller. Some particular laws of deployment/retrieval leading to analytical solutions for the small in-plane and out-of-plane motions of the system are obtained and then these results are extended to a massive tether in Ref. [5]. To fulfill the station-keep control of the rotating TSS along halo orbits, a nonlinear output tracking control scheme based on the h-D technique is proposed in Ref. [6]. This approach overcomes some limitations such as on-line computations of the algebraic Riccati equation and is easy to implement.

The attitude control of a tethered system in space has received extensive attention with several articles published on the subject in recent years. Nohmi [7–9] investigated the arm link to control the TSR's attitude during the deployment phase, and a microgravity experiment was conducted to validate the feasibility of this scheme. In Ref. [10], a nonlinear optimal controller is designed based on an inverse optimal technique to control the attitude of a satellite via tether offset variations. The attitude of the mother satellite is controlled by four tethers, which are connected with the subsatellite as described in the literature [11]. Beda [12] investigated how the attitude

Tethered Space Robot
https://doi.org/10.1016/B978-0-12-812309-6.00008-7

dynamics of a tethered satellite can be controlled for eccentric orbits by simply using the feedback of the pitch angle. The tether tension/length control law was designed to control the attitude of a tethered satellite formation as described in the literature [13]. Chang et al. [14] investigated the attitude dynamics and control method of a three-inline tethered satellite flying formation. Menon and Bombardelli [15] proposed a method to control the position and attitude of the two tethered units using two passive dampers placed at the tether attachment point. Bergamaschi and Bonon [16] studied the coupling between the tether taut string vibrations and the satellite attitude motion. A fault-tolerant nonlinear control design was presented by Godard et al. [17] to control the attitude of a satellite using movement of the tether attachment points, and his method examined cases when tether deployment suddenly stops and tether breakage occurs.

The existing literature all focuses on the control of the attitude or orbit separately, and a few research studies on coordinated control using tethers and thrusters can be found. Moreover, the fuel of the gripper is very limited. Therefore it is of much significance to coordinate the tethers and thrusters to realize the attitude or orbit control and save the fuel consumption at the same time. We propose a novel scheme to realize coordinated control of the orbit and attitude for the TSR simultaneously in this chapter. A mechanism for coordinated control is designed to provide control torques by adjusting the position of the mobile tether attachment point while the tether force and thruster force are also coordinated to achieve tracking control of the optimal approaching trajectory. In this way, the tether force is utilized not only in the orbit control but also in the attitude control. Therefore this novel coordinated control scheme can significantly reduce the fuel consumption for the target approaching phase of the TSR.

8.1 ORBIT AND ATTITUDE DYNAMIC MODEL

As shown in Fig. 8.1, the gripper of a TSR is released from the space platform and approaches a target. To accomplish the task of target visual measurement successfully, the gripper is required to track the desired attitude during the target approaching phase. Meanwhile, the approaching trajectory of the gripper is controlled with the information acquired from the visual measurement.

$\boldsymbol{Ox_t y_t z_t}$ represents the target orbital frame with its origin located at the centroid of the target. The axes of the coordinate are oriented as follows: the x-axis is in the local horizontal direction of the orbital plane, the y-axis

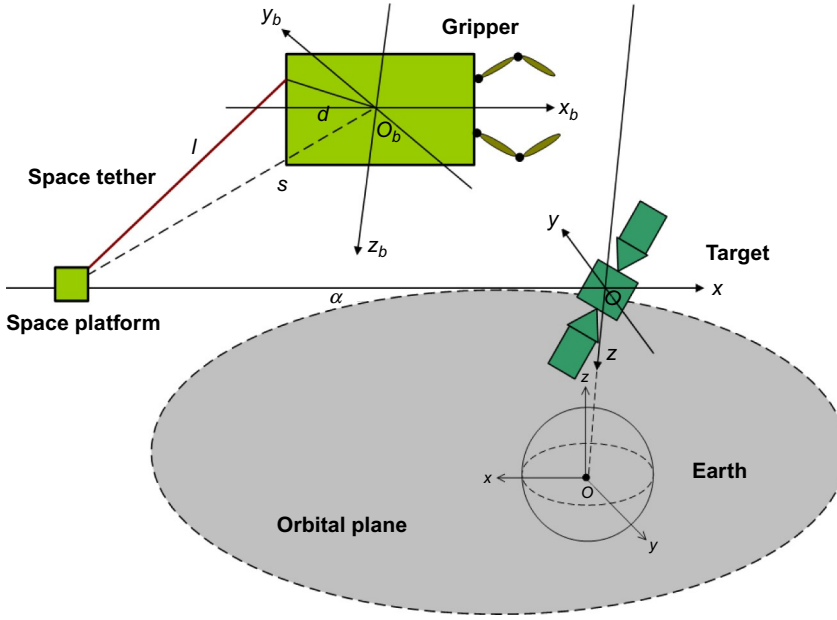

Fig. 8.1 Target approaching phase of TSR system.

is along the orbital normal, and the z-axis is collinear with a line that extends from the center of the Earth to the centroid of the target, which completes a right-handed triad. $\boldsymbol{Ox_by_bz_b}$ is the gripper body frame with its origin at the centroid of the gripper. $\boldsymbol{Ox_py_pz_p}$ is the orbital frame of the space platform.

The following assumptions are made:

(1) The length of the space tether between the space platform and the gripper is hundreds of meters long.

(2) The space tether is inelastic and massless.

(3) The platform can endure the influence of a tether tension from its own thrusters, and its position and attitude can be maintained during the approaching phase of the TSR.

8.1.1 Design of the Mechanism

The coordinated control mechanism is designed to realize the orbit and attitude coordinated control using the space tether simultaneously. Fig. 8.2 shows the coordinated control mechanism, which is located at the base plate plane of the gripper. Four tethers l_a, l_b, l_c, l_d, which come through four holes a, b, c, d are all attached at t called the mobile tether attachment point. The

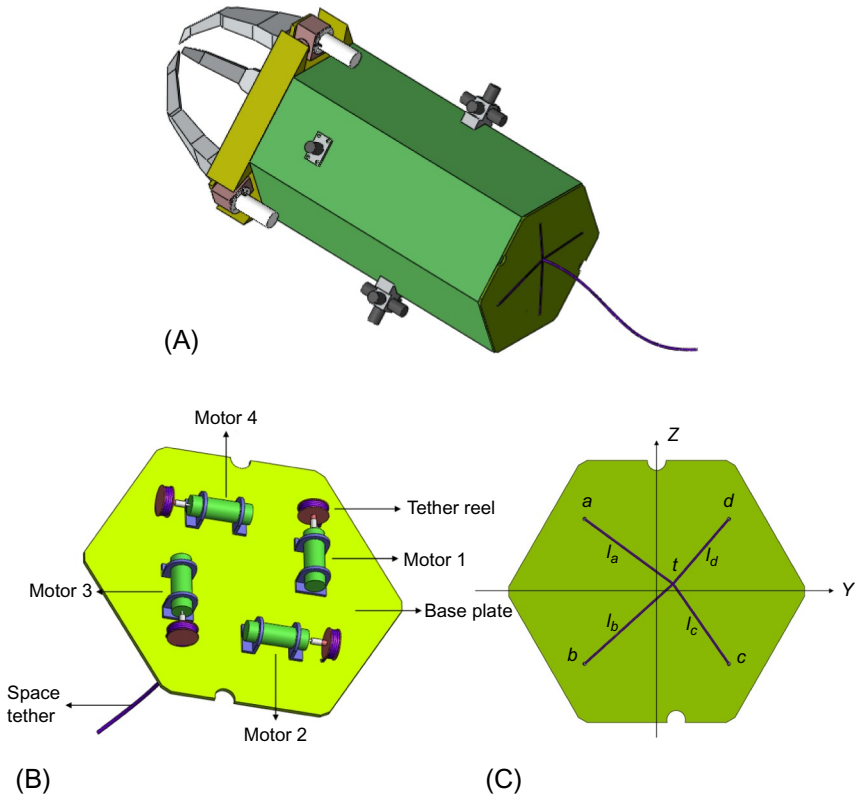

Fig. 8.2 Coordinated control mechanism: (A) diagrammatic sketch of the gripper; (B) mechanism of the tether reel; and (C) back plane of the gripper.

other sides of these four tethers are connected with the tether reels inside the gripper and their lengths are regulated by servo motors. The space tether connecting the TSR and the space platform is also attached at point t.

The tethers of l_a, l_b, l_c, l_d are assumed to be inelastic and massless, and keep taut at the base plate plane of the gripper. The mobile tether attachment point is always at the plane of the gripper and its position can be controlled by adjusting the length of l_a, l_b, l_c, l_d. Different position of t leads to different control torques to the attitude of the gripper. Therefore this principle is used to drive this mechanism to realize the attitude control of the gripper.

Define the position of the gripper in the gripper body frame $\boldsymbol{O}\boldsymbol{x}_b\boldsymbol{y}_b\boldsymbol{z}_b$ as $\boldsymbol{p} = [d \quad \gamma_c \quad z_c]^T$, where d is the distance between the centroid and the base plate plane. The motion of the mobile tether attachment point is constrained in the base plate plane, so d keeps constant. Assume a, b, c, d are located at

four vertexes of a square and their corresponding positions are $[d \ \ -h \ \ h]^T$, $[d \ \ -h \ \ -h]^T$, $[d \ \ h \ \ -h]^T$, $[d \ \ h \ \ h]^T$. Therefore the lengths of each tether l_a, l_b, l_c, l_d are given by:

$$\begin{cases} l_a = \sqrt{(y_c + h)^2 + (z_c - h)^2} \\ l_b = \sqrt{(y_c + h)^2 + (z_c + h)^2} \\ l_c = \sqrt{(y_c - h)^2 + (z_c + h)^2} \\ l_d = \sqrt{(y_c - h)^2 + (z_c - h)^2} \end{cases} \tag{8.1}$$

8.1.2 Attitude Dynamics Model

Assume the gripper is a rigid body and its attitude dynamic equation can be given by the following equation:

$$\boldsymbol{J}\dot{\boldsymbol{\omega}} = -\boldsymbol{\omega}^{\times}\boldsymbol{J}\boldsymbol{\omega} + \boldsymbol{T}_c + \boldsymbol{T}_d \tag{8.2}$$

where $\boldsymbol{\omega} = [\omega_1 \ \ \omega_2 \ \ \omega_3]^T \in \boldsymbol{R}^3$ denotes the absolute angular velocity of the gripper expressed in the body frame $\boldsymbol{O}\boldsymbol{x}_b\boldsymbol{y}_b\boldsymbol{z}_b$. $\boldsymbol{J} \in R^{3\times3}$ is the inertia matrix of the gripper; $\boldsymbol{T}_c$ is the overall control torque and $\boldsymbol{T}_c = \boldsymbol{T}_t + \boldsymbol{T}_l$, where $\boldsymbol{T}_t \in \boldsymbol{R}^3$ denotes the control torque of the gripper and is realized via PWM thrusters, $\boldsymbol{T}_l \in \boldsymbol{R}^3$ represents the control torque generated by the coordinated control mechanism as shown in Fig. 8.2. $\boldsymbol{T}_d \in \boldsymbol{R}^3$ is the attitude disturbance torque. $\boldsymbol{\omega}^{\times}$ is the skew-symmetric matrix of $\boldsymbol{\omega}$ defined as follows:

$$\boldsymbol{\omega}^{\times} = \begin{pmatrix} 0 & -\boldsymbol{\omega}_3 & \boldsymbol{\omega}_2 \\ \boldsymbol{\omega}_3 & 0 & -\boldsymbol{\omega}_1 \\ -\boldsymbol{\omega}_2 & \boldsymbol{\omega}_1 & 0 \end{pmatrix}$$

The kinematics model of the gripper attitude is described by the modified Rodrigues parameter (MRP) [18] as follows:

$$\dot{\boldsymbol{\sigma}} = G(\boldsymbol{\sigma})\boldsymbol{\omega} \tag{8.3}$$

where $\boldsymbol{\sigma} = [\sigma_1 \ \ \sigma_2 \ \ \sigma_3]^T \in R^3$ and $G(\boldsymbol{\sigma})$ is defined as follows:

$$G(\boldsymbol{\sigma}) = \frac{1}{4}\left[\left(1 - \boldsymbol{\sigma}^T\boldsymbol{\sigma}\right)\boldsymbol{I} + 2\boldsymbol{\sigma}^{\times} + 2\boldsymbol{\sigma}\boldsymbol{\sigma}^T\right] \tag{8.4}$$

where $\boldsymbol{I}$ is a 3×3 unit matrix.

The transformation matrix from the orbital frame of the space platform $\boldsymbol{Ox_p y_p z_p}$ to the gripper body frame $\boldsymbol{Ox_b y_b z_b}$ is:

$$\boldsymbol{R} = \boldsymbol{I}_3 - \frac{4(1-\boldsymbol{\sigma}^2)}{(1+\boldsymbol{\sigma}^2)^2}[\boldsymbol{\sigma}^\times] + \frac{8}{(1+\boldsymbol{\sigma}^2)^2}[\boldsymbol{\sigma}^\times]^2 \tag{8.5}$$

For convenience, the relative attitude angles from $\boldsymbol{Ox_p y_p z_p}$ to $\boldsymbol{Ox_b y_b z_b}$ are defined by the Euler angle, the roll angle ϕ, the pitch angle θ, and the yaw angle ψ of the 1-2-3 Euler rotation sequence. The term $\boldsymbol{R}$ can be expressed by ϕ, θ and ψ as follows:

$$\boldsymbol{R} = \begin{bmatrix} \cos\psi\cos\theta & \cos\psi\sin\theta\sin\phi + \sin\psi\cos\phi & -\cos\psi\sin\theta\cos\phi + \sin\psi\sin\phi \\ -\sin\psi\cos\theta & -\sin\psi\sin\theta\sin\phi + \cos\psi\cos\phi & \sin\psi\sin\theta\cos\phi + \cos\psi\sin\phi \\ \sin\theta & -\cos\theta\sin\phi & \cos\theta\cos\phi \end{bmatrix} \tag{8.6}$$

Combine Eqs. (8.5) and (8.6) and three Euler angles ϕ, θ, and ψ can be obtained.

$$\begin{cases} \theta = \arcsin\left(\boldsymbol{R}_{bl}(3,1)\right) \\ \phi = \arctan\left(-\dfrac{\boldsymbol{R}_{bl}(3,2)}{\boldsymbol{R}_{bl}(3,3)}\right) \\ \psi = \arctan\left(-\dfrac{\boldsymbol{R}_{bl}(2,1)}{\boldsymbol{R}_{bl}(1,1)}\right) \end{cases} \tag{8.7}$$

The error attitude MRP $\boldsymbol{\sigma}_e$ and the error attitude angular velocity ω_e of the body frame are defined as follows:

$$\begin{cases} \boldsymbol{\sigma}_e = \boldsymbol{\sigma} \otimes \boldsymbol{\sigma}_d^{1-} \\ \boldsymbol{\omega}_e = \boldsymbol{\omega} - \boldsymbol{\omega}_d \end{cases} \tag{8.8}$$

where $\boldsymbol{\omega}_d$ denotes the desired angular velocity in the body frame and $\boldsymbol{\sigma}_d$ is the desired attitude. The symbol $\otimes$ denotes the MRP multiplication which can be defined as follows:

$$\boldsymbol{\sigma}_1 \otimes \boldsymbol{\sigma}_2^{-1} = \frac{\left(1-\boldsymbol{\sigma}_2^T\boldsymbol{\sigma}_2\right)\boldsymbol{\sigma} + \left(\boldsymbol{\sigma}_1^T\boldsymbol{\sigma}_1 - 1\right)\sigma_2 - 2\boldsymbol{\sigma}_2 \times \boldsymbol{\sigma}_1}{1 + (\boldsymbol{\sigma}_2^T\boldsymbol{\sigma}_2)(\boldsymbol{\sigma}_1^T\boldsymbol{\sigma}_1) + 2\boldsymbol{\sigma}_2^T\boldsymbol{\sigma}_1} \tag{8.9}$$

Substitute Eq. (8.8) into (8.2) and (8.3), and the error attitude dynamic equation and the kinematics equation can be obtained:

$$\begin{cases} \dot{\boldsymbol{\sigma}}_e = G(\boldsymbol{\sigma}_e)\boldsymbol{\omega}_e \\ \boldsymbol{J}\dot{\boldsymbol{\omega}}_e = -\boldsymbol{\omega}^\times \boldsymbol{J}\boldsymbol{\omega} - \boldsymbol{J}\boldsymbol{R}\dot{\boldsymbol{\omega}}_d + \boldsymbol{T}_c + \boldsymbol{T}_l + \boldsymbol{T}_d \end{cases} \tag{8.10}$$

8.1.3 Orbit Dynamic Model

The Hill equation is used to represent the relative orbit motion of the gripper and a target:

$$\begin{cases} \ddot{x}_r - 2n\dot{z}_r = \dfrac{\boldsymbol{u}_x}{m_r} + \dfrac{\boldsymbol{F}_{lx}}{m_r} \\ \ddot{y}_r + n^2 y = \dfrac{\boldsymbol{u}_y}{m_r} + \dfrac{\boldsymbol{F}_{ly}}{m_r} \\ \ddot{z}_r + 2n\dot{x}_r - 3n^2 z_r = \dfrac{\boldsymbol{u}_z}{m_r} + \dfrac{\boldsymbol{F}_{lz}}{m_r} \end{cases} \tag{8.11}$$

where $\begin{bmatrix} x_r & y_r & z_r \end{bmatrix}^T \in \boldsymbol{R}^3$ is the centroid position of the gripper in the target orbital frame $\boldsymbol{Ox_t y_t z_t}$, n denotes the mean orbital angular velocity. $\begin{bmatrix} \boldsymbol{u}_x & \boldsymbol{u}_y & \boldsymbol{u}_z \end{bmatrix}^T \in \boldsymbol{R}^3$ denotes the gripper's thruster force, and $\begin{bmatrix} \boldsymbol{F}_{lx} & \boldsymbol{F}_{ly} & \boldsymbol{F}_{lz} \end{bmatrix}^T \in R^3$ denotes the tether force. m_r is the mass of the gripper.

The position vector of the space platform position in the target orbital frame is defined as $\begin{bmatrix} x_p & y_p & z_p \end{bmatrix}^T \in \boldsymbol{R}^3$, then the relative position between the gripper and the platform is given by:

$$\boldsymbol{s} = \begin{bmatrix} x_r - x_p & y_r - y_p & z_r - z_p \end{bmatrix}^T$$

The position vector between the mobile tether attachment point and the platform is obtained:

$$\boldsymbol{l} = \boldsymbol{s} + \boldsymbol{R}^{-1}\boldsymbol{p} \tag{8.12}$$

Hence, the tether force is:

$$\boldsymbol{F}_l = \begin{bmatrix} \boldsymbol{F}_{lx} & \boldsymbol{F}_{ly} & \boldsymbol{F}_{lz} \end{bmatrix} = -\frac{\boldsymbol{l}}{|\boldsymbol{l}|} T \tag{8.13}$$

where T denotes the tether tension. A tether tension that is too great can strongly influence the space platform and even cause instability of the system; Therefore T should meet the following constraint:

$$T \leq T_{\max} \tag{8.14}$$

Define T_0 as the desired tether tension and ΔT the deviation of the tether tension, then

$$T = T_0 + \Delta T \tag{8.15}$$

The tether control torque in gripper body frame is given by:

$$\boldsymbol{T}_l = \boldsymbol{p} \times (\boldsymbol{R}\boldsymbol{F}_l) \tag{8.16}$$

8.1.4 Task Description of Attitude Control

During the approaching phase, the attitude of the gripper is required to be controlled according to the requirement of certain tasks such as target observation or platform communication. The information of the relative position and relative attitude between the gripper and the target is essential for the target approaching control. Vision measurement is one of the common guiding methods for its relatively low cost and robustness. Successful and continuous vision measurement of a target requires the target to be steadily kept in the field of view. Therefore the aim of the attitude control is assumed to keep the gripper right in the center of view. The corresponding desired attitude can be obtained by the following steps.

The desired attitude for vision measurement is related to the position of the gripper. Therefore the corresponding desired Euler angles from the gripper's position $[x_r \quad y_r \quad z_r]^T$ is obtained at first:

$$\begin{cases} \varphi = 0 \\ \theta = \text{ac tan}\left(\dfrac{z_r}{x_r}\right) \\ \psi = \text{ar tan}\left(\dfrac{y_r}{\sqrt{{x_r}^2 + {z_r}^2}}\right) \end{cases} \tag{8.17}$$

where the pitch θ and yaw ψ have great influences on the vision measurement of target while the influence of roll φ is very small. Therefore the desired roll angle is set to be zero.

The range of the plane for the motion of the mobile tether attachment point is limited, therefore z_c and y_c satisfy the following constraints:

$$\begin{cases} -h \le z_c \le h \\ -h \le y_c \le h \end{cases} \tag{8.18}$$

As a result, the maximum attitude controlled by the mechanism is obtained:

$$\begin{cases} \theta_{\max} = \text{ac tan}\left(\dfrac{h}{d}\right) \\ \psi_{\max} = \text{ar tan}\left(\dfrac{h}{d}\right) \end{cases} \tag{8.19}$$

The desired MRP attitude can be acquired by the following ways. The transformation matrix $\boldsymbol{R}_d$ of the desired attitude is given by:

$$\boldsymbol{R}_d = \begin{bmatrix} \cos\psi\cos\theta & \cos\psi\sin\theta\sin\varphi + \sin\psi\cos\varphi & -\cos\psi\sin\theta\cos\varphi + \sin\psi\sin\varphi \\ -\sin\psi\cos\theta & -\sin\psi\sin\theta\sin\varphi + \cos\psi\cos\varphi & \sin\psi\sin\theta\cos\varphi + \cos\psi\sin\varphi \\ \sin\theta & -\cos\theta\sin\varphi & \cos\theta\cos\varphi \end{bmatrix} \tag{8.20}$$

From the transformation matrix $\boldsymbol{R}_d$, the rotating angle α, and the Euler axis $\boldsymbol{e} = \begin{pmatrix} e_x & e_y & e_z \end{pmatrix}^T$ are:

$$\begin{cases} \cos\alpha = \left(\boldsymbol{R}_{lp11} + \boldsymbol{R}_{lp22} + \boldsymbol{R}_{lp33} - 1\right)/2 \\ e_x = \left(\boldsymbol{R}_{lp23} - \boldsymbol{R}_{lp32}\right)/(2\sin\alpha) \\ e_y = \left(\boldsymbol{R}_{lp31} - \boldsymbol{R}_{lp13}\right)/(2\sin\alpha) \\ e_z = \left(\boldsymbol{R}_{lp12} - \boldsymbol{R}_{lp21}\right)/(2\sin\alpha) \end{cases} \tag{8.21}$$

According to the definition of the MRP, $\boldsymbol{\sigma}_d$ is obtained as follows:

$$\boldsymbol{\sigma}_d = \tan\frac{\alpha}{4}\boldsymbol{e} \tag{8.22}$$

Also, the desired angular velocity is defined as $\boldsymbol{\omega}_d = \begin{bmatrix} 0 & 0 & 0 \end{bmatrix}^T$

8.2 STRATEGY DESIGN OF THE COORDINATED CONTROLLER

The aim of our coordinated control design is to realize the coordinated control of the position and attitude of the gripper using the tether tension at the same time. However, the tether tension must satisfy some constraints when the mechanism is utilized for the attitude control. Therefore the attitude coordinated controller is designed first. Then the approaching trajectory is planned according to the tether tension requirement of the attitude control and the corresponding orbit coordinated controller is designed.

8.2.1 Attitude Coordinated Controller Design

Before the design of the attitude coordinated controller, the following two points must be noted:

(1) The mechanism could only provide control torques for the pitch and yaw motions of the gripper. Therefore the proper controller of the mechanism should be designed to drive the mechanism.

(2) The roll of the gripper cannot be controlled by the mechanism and is coupled with the other two axes of motions. Therefore the roll motion is considered to be controlled using the thruster.

The sliding mode control method is recognized as an efficient tool for designing robust controllers for nonlinear dynamic plants under uncertainty conditions. Therefore the sliding mode control is adopted to reduce the influence of the uncertainty in the tether tension.

The error attitude dynamic equation is given by Eq. (8.10). Defined the sliding surface as $\boldsymbol{S}=\boldsymbol{\omega}_e+c\boldsymbol{\sigma}_e$, where $c>0$

The sliding mode controller is designed as:

$$\boldsymbol{T}_c=\boldsymbol{\omega}^{\times}\boldsymbol{J}\boldsymbol{\omega}+\boldsymbol{J}\dot{\boldsymbol{\omega}}_d-c\boldsymbol{J}G(\boldsymbol{\sigma}_e)\boldsymbol{\omega}_e+\lambda\,\mathrm{sgn}(\boldsymbol{S}) \tag{8.23}$$

where $\lambda>0$

Choose $V=\frac{1}{2}\boldsymbol{S}^T\boldsymbol{J}\boldsymbol{S}$ as the Lyapunov function and the time derivative of V is:

$$\begin{aligned}\dot{V}&=\boldsymbol{S}^T\boldsymbol{J}\dot{\boldsymbol{S}}\\&=\boldsymbol{S}^T\boldsymbol{J}(\dot{\boldsymbol{\omega}}_e+c\dot{\boldsymbol{\sigma}}_e)\end{aligned} \tag{8.24}$$

Substitute Eq. (8.10) into (8.24), and one can obtain:

$$\dot{V}=\boldsymbol{S}^T(\boldsymbol{T}_c+\boldsymbol{T}_d-\boldsymbol{\omega}^{\times}\boldsymbol{J}\boldsymbol{\omega}-\boldsymbol{J}\dot{\boldsymbol{\omega}}_d+c\boldsymbol{J}G(\boldsymbol{\sigma}_e)\boldsymbol{\omega}_e)$$

From Eqs. (8.13), (8.15)–(8.16), the tether control torque is given by:

$$\boldsymbol{T}_l=\boldsymbol{p}\times\left[\boldsymbol{R}\left(-\frac{\boldsymbol{l}}{|\boldsymbol{l}|}(T_0+\Delta T)\right)\right]$$

Substituting $\boldsymbol{T}_c=\boldsymbol{T}_t+\boldsymbol{T}_l=\boldsymbol{T}_t+\boldsymbol{p}\times\left[\boldsymbol{R}\left(-\frac{\boldsymbol{l}}{|\boldsymbol{l}|}T_d\right)\right]$ into $\dot{V}$ yields:

$$\dot{V}=\boldsymbol{S}^T[f(\Delta T)-\lambda\,\mathrm{sgn}(\boldsymbol{S})]$$

where $\boldsymbol{f}(\Delta T)=\boldsymbol{p}\times\left[\boldsymbol{R}\left(-\frac{\boldsymbol{l}}{|\boldsymbol{l}|}\Delta T\right)\right]+\boldsymbol{T}_d$, the fluctuation of the tether tension ΔT, and the space disturbance are bounded, suggesting that $\boldsymbol{f}$ is also bounded. Assuming $\begin{cases}\Delta_{\max}=\|\boldsymbol{f}\|_{\infty}\\ \boldsymbol{f}=[\Delta_1\quad\Delta_2\quad\Delta_3]^T\end{cases}$ and setting $\lambda=\Delta_{\max}+\delta$ in which δ is an arbitrary positive number, one can derive:

$$\begin{aligned}\dot{V}&=\sum_{i=1}^{3}\boldsymbol{S}_i{}^T[-(\Delta_{\max}+\delta)\,\mathrm{sgn}(\boldsymbol{S}_i)+\Delta_i]\\&=\sum_{i=1}^{3}\boldsymbol{S}_i{}^T[-\delta\,\mathrm{sgn}(\boldsymbol{S}_i)-\Delta_{\max}\,\mathrm{sgn}(\boldsymbol{S}_i)+\Delta_i]\\&=-\sum_{i=1}^{3}\boldsymbol{S}_i{}^T\delta\,\mathrm{sgn}(\boldsymbol{S}_i)+\sum_{i=1}^{3}\left[-\Delta_{\max}\boldsymbol{S}_i{}^T\,\mathrm{sgn}(\boldsymbol{S}_i)+\Delta_i\boldsymbol{S}_i{}^T\right]\\&\le-\sum_{i=1}^{3}\boldsymbol{S}_i{}^T\delta\,\mathrm{sgn}(\boldsymbol{S}_i)\le 0\end{aligned}$$

$V > 0$ and $\dot{V} \leq 0$, so it is believed that an asymptotically stable system meets the sliding condition.

Chattering in the control system may occur for the existence of the sign function in Eq. (8.23). To solve this problem, the sign function can be modified into the saturation functions:

$$sat(\boldsymbol{S}_i, \varepsilon) = \begin{cases} 1 & \boldsymbol{S}_i > \varepsilon \\ \boldsymbol{S}_i/\varepsilon & -\varepsilon \leq \boldsymbol{S}_i \leq \varepsilon \\ -1 & \boldsymbol{S}_i < -\varepsilon \end{cases} \tag{8.25}$$

where $i = 1,2,3$ and ε is a positive number.

The desired attitude control torque T_c can be calculated by the sliding mode controller of Eq. (8.23). However, the method to drive the mechanism to generate such desired torques will be designed afterwards.

The tether tension vector in the gripper body frame $\boldsymbol{O}\boldsymbol{x}_b\boldsymbol{y}_b\boldsymbol{z}_b$ is $\boldsymbol{F}_{lb} = \boldsymbol{F}_l\boldsymbol{R}$ and the tether torques caused by such tether tension are given by:

$$\left[\gamma_c\boldsymbol{F}_{lbz} - z_c\boldsymbol{F}_{lby} \quad z_c\boldsymbol{F}_{lbx} - d\boldsymbol{F}_{lbz} \quad d\boldsymbol{F}_{lby} - \gamma_c\boldsymbol{F}_{lbx}\right] \tag{8.26}$$

From Eq. (8.26), we can obtain the position of the mobile tether attachment point by which the mechanism can generate the desired control torques for the pitch and yaw motions:

$$\begin{cases} z_c = \left(\boldsymbol{T}_{cy} + d\boldsymbol{F}_{lbz}\right)/\boldsymbol{F}_{lbx} \\ \gamma_c = \left(d\boldsymbol{F}_{lby} - \boldsymbol{T}_{cz}\right)/\boldsymbol{F}_{lbx} \end{cases} \tag{8.27}$$

where $\boldsymbol{T}_{cy}$ and $\boldsymbol{T}_{cz}$ are two elements of the desired control torque T_c in Eq. (8.23).

The constraints of the position of mobile tether attachment point must be satisfied:

$$\begin{cases} \gamma_{c\min} < \gamma_c < \gamma_{c\max} \\ z_{c\min} < z_c < z_{c\max} \end{cases} \tag{8.28}$$

Besides, we must notice that a disturbing torque, $\gamma_c\boldsymbol{F}_{lbz} - z_c\boldsymbol{F}_{lby}$, also exists in Eq. (8.26). However, this torque is usually very small. Therefore the additional fuel for suppression of this disturbing torque is very small compared with the fuel reduction of the other two axes using the coordinated control mechanism,. Therefore thrusters are utilized to control the roll motion and eliminate the influence of this disturbing torque.

Also, the following problems should be considered:

(1) Considering the capacity of the actual coordinated control mechanism to track the position of the mobile tether attachment point in

Eq. (8.27), we can adjust the value of parameter c to reduce the required control torques as much as possible on the condition of attitude stability. With this method, the coordinated control mechanism can provide the required control torques promptly.

(2) From Eq. (8.27), we must notice that the tether tension should exist all the time to generate the required attitude control torque during the use of the mechanism. A tether tension that is too small may lead to inadequate control torque, which should be avoided. Moreover, given that the tension along the tether cannot be controlled very precisely, the tether tension should not vary severely.

8.2.1 Coordinated Tracking Controller Design

Given the requirement of the tether tension along the tether and the difficulty to precisely generate the required tether tension, a constant value of tether tension T is designed for the optimal approaching trajectory of the gripper. This strategy to deal with the tether tension is relatively more easily accomplished and satisfies the conditions for the mechanism to function properly. Moreover, the influences of the attitude of the gripper on the space tether force and the position are relatively limited, so we decouple the attitude and orbit to design the approaching trajectory without considering the attitude.

The relative orbit dynamics model of the gripper and the target in Eq. (8.11) can be rewritten as:

$$\begin{cases} \ddot{x}_r - 2n\dot{z}_r = \dfrac{\boldsymbol{u}_x}{m_r} - \dfrac{T\left(x_r - x_p\right)}{m_r\sqrt{\left(x_r - x_p\right)^2 + \left(y_r - y_p\right)^2 + \left(z_r - z_p\right)^2}} \\ \ddot{y}_r + n^2 y = \dfrac{\boldsymbol{u}_y}{m_r} - \dfrac{T\left(y_r - y_p\right)}{m_r\sqrt{\left(x_r - x_p\right)^2 + \left(y_r - y_p\right)^2 + \left(z_r - z_p\right)^2}} \\ \ddot{z}_r + 2n\dot{x}_r - 3n^2 z_r = \dfrac{\boldsymbol{u}_z}{m_r} - \dfrac{T\left(z_r - z_p\right)}{m_r\sqrt{\left(x_r - x_p\right)^2 + \left(y_r - y_p\right)^2 + \left(z_r - z_p\right)^2}} \end{cases} \tag{8.29}$$

where $\begin{bmatrix} x_p & y_p & z_p \end{bmatrix}^T \in R^3$ is the centroid position of the space platform in the target orbital frame $\boldsymbol{Ox_t y_t z_t}$.

The fuel of the gripper is limited. Therefore minimal fuel consumption is preferential and the approaching time t_f is not optimized. The trajectory optimization performance index $\boldsymbol{J}_1$ is written as:

$$\boldsymbol{J}_1 = \int_{t_0}^{t_f} \left(\boldsymbol{u}_x{}^2 + \boldsymbol{u}_y{}^2 + \boldsymbol{u}_z{}^2 \right) dt \tag{8.30}$$

Define the state variables as $\boldsymbol{X} = [x_r \;\; y_r \;\; z_r \;\; \dot{x}_r \;\; \dot{y}_r \;\; \dot{z}_r]^T$ and make the optimal trajectory design problem well-defined, the path constraints are expressed as follows:

$$\boldsymbol{X}_{\min} \le \boldsymbol{X} \le \boldsymbol{X}_{\max} \tag{8.31}$$

where $\boldsymbol{X}_{\min}$ and $\boldsymbol{X}_{\max}$ are the minimum and maximum of the state variables separately.

Define the control variables as $\boldsymbol{u} = [\boldsymbol{u}_x \;\; \boldsymbol{u}_y \;\; \boldsymbol{u}_z]^T$, and control constraints must be enforced because the thrusters control forces are bounded:

$$-\boldsymbol{u}_{\max} \le \boldsymbol{u} \le \boldsymbol{u}_{\max} \tag{8.32}$$

Combining Eqs. (8.17) and (8.19) yields:

$$\begin{cases} \dfrac{z_r}{x_r} \le \dfrac{h}{d} \\ \dfrac{y_r}{\sqrt{x_r{}^2 + z_r{}^2}} \le \dfrac{h}{d} \end{cases} \tag{8.33}$$

Eq. (8.33) represents the requirement for the attitude control during the task of the target vision measurement. Thus the basic task is now to design an optimal trajectory satisfying differential constraints in Eq. (8.30), control constraints in Eq. (8.33), path constrains in Eqs. (8.32) and (8.33), and at the same time making the performance index in Eq. (8.31) as small as possible.

The optimal approaching trajectory of the TSR is now designed by a pseudospectral method. The pseudospectral method in the trajectory optimization is a special scheme, which transcribes a continuous dynamic optimization problem to an NLP problem. The various orthogonal polynomials utilized by the pseudospectral method are all defined in the normalized domain $[-1 \;\; 1]$. First, the time domain is transformed by introducing the following equation:

$$\tau = \frac{2t}{t_f - t_0} - \frac{t_f + t_0}{t_f - t_0}$$

where $\tau \in [-1,1]$ is the normalized time. Thus the dynamics of the operational robot in Eq. (8.29) can be transformed into:

$$\frac{d}{d\tau}\boldsymbol{X} = \frac{t_f - t_0}{2}\boldsymbol{f}(\boldsymbol{X}, \boldsymbol{u}, \tau)$$

It can approximate the state variables $\boldsymbol{X}$ by the Lagrange interpolation. Then, the state variables $\boldsymbol{X}$ can be written as:

$$\boldsymbol{X}(\tau) = \sum_{i=0}^{M} L_i(\tau)\boldsymbol{X}(\tau_i)$$

where $L_i(\tau) = \prod_{j=0, j\neq i}^{M} \frac{\tau - \tau_j}{\tau_i - \tau_j}$ is the Lagrange interpolation polynomial based on Legendre-Gauss (LG) point τ_h, $h = 1,2,\ldots,M$, and point $\tau_0 = -1$ is appended by the Gauss pseudospectral method. And the LG points τ_h are the roots of:

$$P_M(\tau) = \frac{1}{2^M M!}\frac{d^M}{d\tau^M}\left[\left(\tau^2 - 1\right)^M\right] = 0$$

However, the state variables $\boldsymbol{X}(\tau)$ do not contain the discrete point at the operational time $\tau_f = 1$. Thus the final variable can be discretized and approximated via the Gauss quadrature.

$$\boldsymbol{X}(\tau_f) - \boldsymbol{X}(\tau_0) - \frac{t_f - t_0}{2}\sum_{i=1}^{M}\omega_i \boldsymbol{f}\left(\boldsymbol{X}(\tau_i), \boldsymbol{U}(\tau_i), \tau_i; t_0, t_f\right) = 0 \tag{8.34}$$

where $\omega_i = \frac{2}{(1-\tau_i^2)\left[\dot{P}_M(\tau_i)\right]^2}$, $i = 1,2,\ldots,M$ are the Gauss weights, $\boldsymbol{U}(\tau_i)$ are an approximation of discrete control force. The control variables $\boldsymbol{u}$ are then approximated by the Lagrange interpolation:

$$\boldsymbol{u}(\tau) = \sum_{i=1}^{M} \widetilde{L}_i(\tau)\boldsymbol{U}(\tau_i)$$

where $\widetilde{L}_i(\tau) = \prod_{j=1, j\neq i}^{M} \frac{\tau - \tau_j}{\tau_i - \tau_j}$ is the Lagrange interpolation polynomial based on the Legendre-Gauss (LG) point τ_h, $h = 1,2,\ldots,M$

The derivatives of the state variables $\boldsymbol{X}(\tau)$ are estimated by differentiating Eq. (8.29):

$$\frac{d\boldsymbol{X}(\tau_k)}{d\tau}=\sum_{i=0}^{M}\dot{L}_i(\tau_k)\boldsymbol{X}(\tau_i)=\sum_{i=0}^{M}D_{ki}\boldsymbol{X}(\tau_i),\quad (k=1,2,\ldots,M) \tag{8.35}$$

where $D_{ki}=\dot{L}_i(\tau_k)=\sum_{l=0}^{M}\frac{\prod_{j=0,j\neq i,l}^{M}(\tau_k-\tau_j)}{\prod_{j=0,j\neq i}^{M}(\tau_i-\tau_j)}$, which are the element of the $M\times(M+1)$ differentiation matrix $\boldsymbol{D}$.

The relative dynamics of the gripper can be approximated by imposing it at some specific nodes. At these nodes, the following equations are satisfied:

$$R_k\equiv\sum_{i=0}^{M}D_{ki}X_i-\frac{t_f-t_0}{2}f\left(X_k,U_k,\tau_k;t_0,t_f\right)=0,\quad (k=1,\ldots,M) \tag{8.36}$$

Thus the algebraic constrains are imposed by the LG point τ_k, $k=1,2,\ldots,M$. And the boundary constraints, path constraints, and control constraints are written directly as:

$$\boldsymbol{X}(-1)=\boldsymbol{X}_0,\quad \boldsymbol{\Phi}(\boldsymbol{X}(1))=0 \tag{8.37}$$

$$\boldsymbol{X}_{\min}\le\boldsymbol{X}(\tau_k)\le\boldsymbol{X}_{\max} \tag{8.38}$$

$$-u_{\max}\le u(\tau_k)\le u_{\max} \tag{8.39}$$

The energy optimal performance index J_1 is discretized as:

$$J_1=\frac{t_f-t_0}{2}\int_{-1}^{1}\boldsymbol{u}^T(\tau)\boldsymbol{u}(\tau)d\tau=\frac{t_f-t_0}{2}\sum_{k=1}^{M}\boldsymbol{U}^T(\tau_k)\boldsymbol{U}(\tau_k)\omega_k \tag{8.40}$$

Therefore the cost function in Eq. (8.40) and various constraints in Eqs. (8.34), (8.36)–(8.39) finally formulate the original continuous optimization problem as an NLP. The optimized state variables $\boldsymbol{X}(\tau_i)$, $i=0,1,2,\ldots,M$ and the control force $\boldsymbol{U}(\tau_k)$, $k=1,2\ldots,M$. These parameters can be solved by SNOPT optimization algorithm [19]. And the optimal discrete control force $\boldsymbol{U}(\tau_k)$ and optimal discrete trajectory $\boldsymbol{X}(\tau_i)$ are obtained. The continuous optimal control force and trajectory are obtained via the Lagrange interpolation toward discrete points.

Then, the coordinated controller to track the optimal approaching trajectory will be designed. To suppress the influence of the tether tension fluctuation around the desired tension, a robust coordinated controller is required to compensate this undesired influence.

To reduce the influence of the uncertainty in the tether tension, a sliding mode method is used in the controller design. However, the robustness of the traditional sliding mode control is guaranteed only after the system state reaches the sliding surface but not during the reaching phase while the uncertainty in the tether tension exists all the time. Therefore a time-varying sliding mode proposed in Ref. [20], in which the system initial state is on the sliding surface to eliminate the reaching phase, will be used in the design of our coordinated controller.

Assume $\begin{cases} \boldsymbol{F}_x = \boldsymbol{u}_x + \boldsymbol{F}_{lx} \\ \boldsymbol{F}_y = \boldsymbol{u}_y + \boldsymbol{F}_{ly} \\ \boldsymbol{F}_z = \boldsymbol{u}_z + \boldsymbol{F}_{lz} \end{cases}$, and Eq. (8.11) can be rewritten as:

$$\begin{cases} \ddot{x}_r - 2n\dot{z}_r = \dfrac{\boldsymbol{F}_x}{m_r} \\ \ddot{y}_r + n^2 y_r = \dfrac{\boldsymbol{F}_y}{m_r} \\ \ddot{z}_r + 2n\dot{x}_r - 3n^2 z_r = \dfrac{\boldsymbol{F}_z}{m_r} \end{cases} \tag{8.41}$$

where

$$\boldsymbol{A} = \begin{pmatrix} 0 & 0 & 0 & 1 & 0 & 0 \\ 0 & 0 & 0 & 0 & 1 & 0 \\ 0 & 0 & 0 & 0 & 0 & 1 \\ 0 & 0 & 0 & 0 & 0 & 2n \\ 0 & -n^2 & 0 & 0 & 0 & 0 \\ 0 & 0 & 3n^2 & -2n & 0 & 0 \end{pmatrix}, \quad \boldsymbol{B} = \begin{pmatrix} 0 & 0 & 0 \\ 0 & 0 & 0 \\ 0 & 0 & 0 \\ 1 & 0 & 0 \\ 0 & 1 & 0 \\ 0 & 0 & 1 \end{pmatrix}, \quad \boldsymbol{x} = \begin{pmatrix} x_r \\ y_r \\ z_r \\ x_r' \\ y_r' \\ z_r' \end{pmatrix},$$

$$\boldsymbol{F} = \begin{pmatrix} \boldsymbol{F}_x \\ \boldsymbol{F}_y \\ \boldsymbol{F}_z \end{pmatrix}$$

Define the varying sliding surface as:

$$\boldsymbol{S} = \boldsymbol{C}\boldsymbol{x}_e + \begin{cases} c_1 t^2 + c_2 t + c_3, t \le T \\ 0, t \ge T \end{cases} \tag{8.42}$$

where $T > 0$ is the switching time, $\boldsymbol{C} \in \boldsymbol{R}^{3\times 6}$ is the slope of the sliding surface and both parameters are constant. $\boldsymbol{x}_d$ denotes the desired optimal trajectory and $\boldsymbol{x}_e = \boldsymbol{x}_d - \boldsymbol{x}$ the trajectory tracking error of the TSR. Let $\boldsymbol{c}_1, \boldsymbol{c}_2, \boldsymbol{c}_3 \in \boldsymbol{R}^{3\times 1}$ be constant vectors, such that

(1) The initial value of the system belongs to the sliding surface defined by Eq. (8.42):

$$\boldsymbol{C}\boldsymbol{x}_e(0) + \boldsymbol{c}_3 = 0 \tag{8.43}$$

(2) The right side of Eq. (8.42) is continuous with its derivative at time T:

$$\begin{cases} \boldsymbol{c}_1 T^2 + \boldsymbol{c}_2 T + \boldsymbol{c}_3 = 0 \\ 2\boldsymbol{c}_1 T + \boldsymbol{c}_2 = 0 \end{cases} \tag{8.44}$$

Combining Eqs. (8.43) and (8.44) yields:

$$\begin{cases} \boldsymbol{c}_1 = -[\dot{\boldsymbol{x}}(0) + k\boldsymbol{x}(0)]/T^2 \\ \boldsymbol{c}_2 = 2[\dot{\boldsymbol{x}}(0) + k\boldsymbol{x}(0)]/T \\ \boldsymbol{c}_3 = -\dot{\boldsymbol{x}}(0) - k\boldsymbol{x} \end{cases} \tag{8.45}$$

The coordinated controller based on the time-varying sliding mode control is designed as:

$$\boldsymbol{F} = \begin{cases} (\boldsymbol{CB})^{-1}\left(-\boldsymbol{C}\boldsymbol{x}_d' + \boldsymbol{CAx} - 2\boldsymbol{c}_1 t - \boldsymbol{c}_2 + \mathrm{sgn}(\boldsymbol{S})\right), & t \le T \\ (\boldsymbol{CB})^{-1}\left(-\boldsymbol{C}\boldsymbol{x}_d' + \boldsymbol{CAx} + \mathrm{sgn}(\boldsymbol{S})\right), & t \ge T \end{cases} \tag{8.46}$$

where

$$M = \begin{cases} (CB)^{-1}, & CB > 0 \\ -(CB)^{-1}, & CB < 0 \end{cases} \quad \text{and} \quad M > 0.$$

By choosing $V = \frac{1}{2} S^T M S$ as the Lyapunov function, the time derivative of V is

$$\begin{aligned} \dot{V} &= S^T M \dot{S} \\ &= S^T M \begin{cases} C\dot{x}_e + 2c_1 t + c_2, & t \le T \\ C\dot{x}_e, & t \ge T \end{cases} \\ &= S^T M \begin{cases} C(\dot{x}_d - \dot{x}) + 2c_1 t + c_2, & t \le T \\ C(\dot{x}_d - \dot{x}), & t \ge T \end{cases} \\ &= S^T M \begin{cases} C\dot{x}_d - C(Ax + BF) + 2c_1 t + c_2, & t \le T \\ C\dot{x}_d - C(Ax + BF), & t \ge T \end{cases} \\ &= S^T M \begin{cases} C\dot{x}_d - CAx - CBF + 2c_1 t + c_2, & t \le T \\ C\dot{x}_d - CAx - CBF, & t \ge T \end{cases} \end{aligned} \tag{8.47}$$

Substituting Eq. (8.46) into (8.47), can be obtained:

$$\dot{V} = -S^T M \,\mathrm{sgn}(S) < 0 \tag{8.48}$$

$V > 0$ and $\dot{V} < 0$, so it is believed that an asymptotically stable system meets the sliding condition.

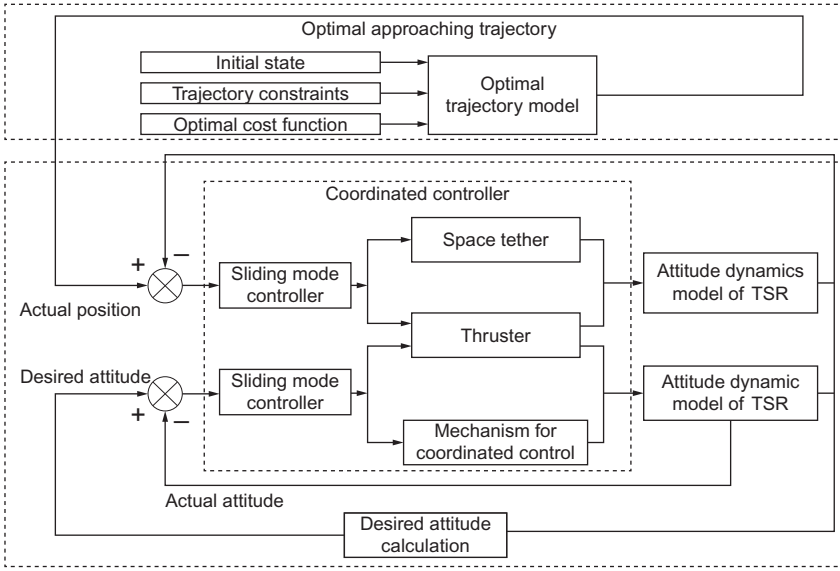

Fig. 8.3 Block diagram of the coordinated controllers.

The switching time T in the control law can be optimized, and time and fuel consumption can be considered in the corresponding cost function.

The forces of the thruster are given by:

$$\begin{cases} u_x = F_x - F_{lx} \\ u_y = F_y - F_{ly} \\ u_z = F_z - F_{lz} \end{cases} \tag{8.49}$$

Fig. 8.3 shows the block diagram of the coordinated controller for the target approaching process of the TSR.

8.3 NUMERICAL SIMULATION

Numerical simulation includes two sections: Section 8.3.1 presents an optimal trajectory with constant tether tension to satisfy the requirement of tether tension for the mechanism. Then the proposed coordinated controller is verified in Section 8.3.2.

8.3.1 Trajectory Planning with Constant Tether Tension

The initial position of the gripper for the trajectory planning is assumed to be $(-190,0,0)$ m with an initial velocity of $(1.5,0,0.15)$ m/s. The desired

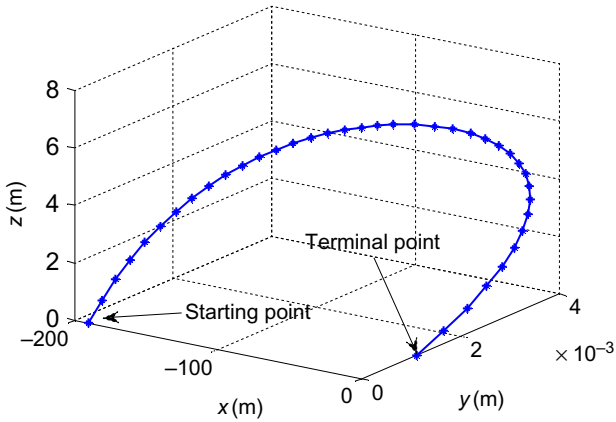

Fig. 8.4 Optimal approaching trajectory of the gripper.

terminal point is $(0,0,0)$ m and the final relative velocity is $(0,0,0)$ m/s according to the requirement of capture mission. The maximum thruster force of the gripper is 0.5 N, and the constant tether tension T is set to be 0.2 N.

The optimal approaching trajectory of the TSR solved by the pseudospectral method is shown in Fig. 8.4. It can be seen that the maximum offset along the z-axis is less than 8 m. Note that the offset along the y-axis are kept within ± 0.01 m, suggesting that the motion of the gripper is only in the orbital plane. Fig. 8.5 illustrates the corresponding control force of the optimal approaching trajectory.

8.3.2 Simulation Results of the Coordinated Control

Assume the initial position of the space platform is $[-200 \quad 0 \quad 0]^T$ m, which is kept stable during the approaching phase. The gripper is released and approaching towards the target from $-$V bar. The main simulation parameters are shown in Table 8.1.

The thrusters are assumed to have a constant control force of 0.5 N and a constant control torque of 0.05 Nm when the corresponding thrusters are turned on and work in PWM mode with a control cycle of 250 ms. The parameters of the proposed mechanism for coordinated control are shown in Table 8.2. The deviation of the tether tension ΔT is assumed to be $40\sin(2\pi t)$ mN. The simulation results are as follows.

Figs. 8.6 and 8.7 show the position tracking results of the gripper and the corresponding tracking errors. It can be seen that the proposed coordinated

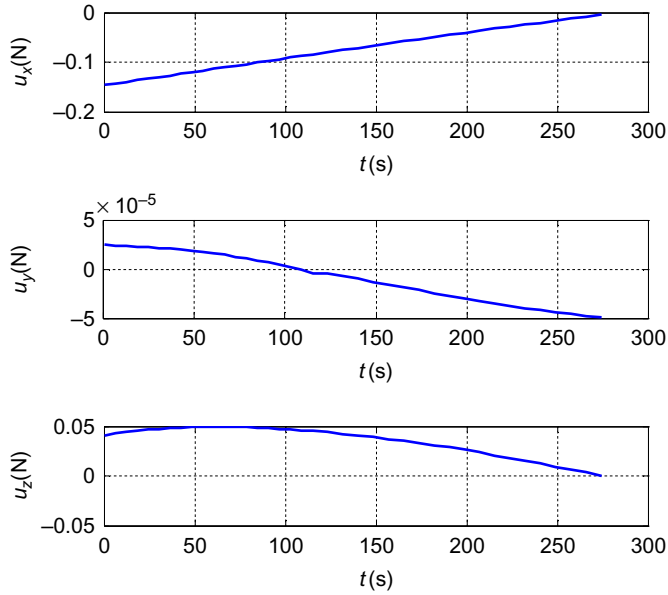

Fig. 8.5 Control force for the optimal approaching trajectory.

Table 8.1 Initial parameters of the gripper

Parameters	Initial values
m_r	50 kg
$\boldsymbol{J}$	diag(8,9.6,8.8) kg m
n	0.0011 rad/s
$(x_r \quad y_r \quad z_r)^T$	$(-191,0.2,-0.1)^T$ m
$(\dot{x}_r \quad \dot{y}_r \quad \dot{z}_r)^T$	$(1.55,0,\text{-}0.18)^T$ m/s
$\boldsymbol{\sigma}$	$(0.02,0.03,0.03)^T$
$\boldsymbol{\omega}$	$(0,0,0)^T$ degrees/s

Table 8.2 Configuration of the mechanism

Parameters	Initial values	Parameters	Initial values
d	0.5 m	h	0.2 m
a	$(-0.5,-0.2,0.2)^T$m	b	$(-0.5,-0.2,-0.2)^T$m
c	$(-0.5,0.2,-0.2)^T$m	d	$(-0.5,0.2,0.2)^T$m

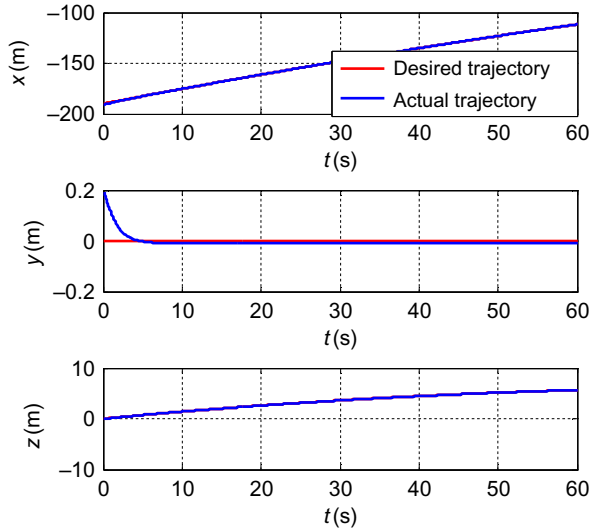

Fig. 8.6 Tracking control result of position.

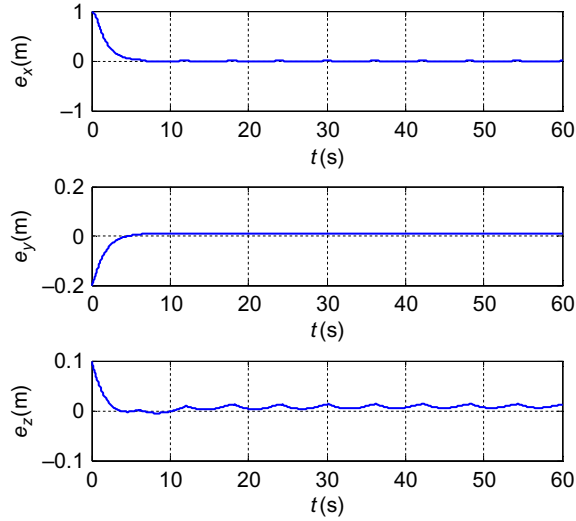

Fig. 8.7 Tracking errors of the position.

position controller can eliminate the influence of the tether tension fluctuation. The tracking errors of the position are substantially eliminated after about 10 s and become less than 5 cm, which satisfies the position requirement of the target approaching task. Besides, tracking precision that is too high is not necessary and may lead to additional fuel consumption. Fig. 8.8 is the linear velocity of the gripper.

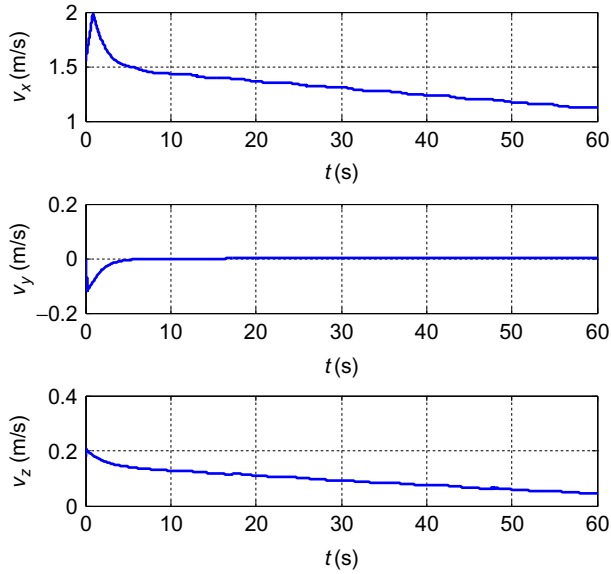

Fig. 8.8 Velocity of the gripper.

The gripper approaches target from –V bar, so the tether force is mainly along the x-axis as illustrated in Fig. 8.9. Fig. 8.10 is the thruster force of the gripper.

To demonstrate the advantages of the coordinated controller proposed in this chapter, an additional simulation using only thruster force is also carried out for comparison. The fuel consumption of these two methods is shown in Fig. 8.11. The final fuel consumption of the coordinated control is 2.322, while that of the thruster control is approximately 126.2% higher at 5.252, which clearly demonstrates that the proposed coordinated control could efficiently reduce the fuel consumption.

Figs. 8.12 and 8.13 provide the simulation results of the three-axis attitude σ, and the corresponding Euler angles (1-2-3). From Figs. 8.12 and 8.13, we can see that the convergence time of the coordinated controller is approximately 20 s and the actual attitude can realize the track control the desired attitude. The maximum tracking error of the attitude is 0.4 degrees in the yaw motion, which is acceptable for the gripper during the approaching phase. Fig. 8.14 is the angular velocity of the gripper. The maximum angular velocity is about −1 degrees/s in the roll and pitch motions, which is eliminated quickly.

The position of the mobile tether attachment point can be seen in Fig. 8.15 and the corresponding trajectory in the back plane of the gripper

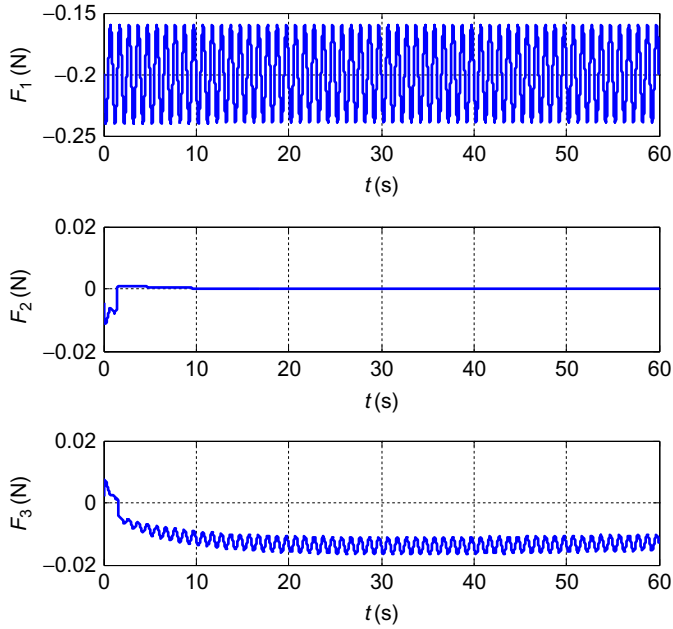

Fig. 8.9 Tether force.

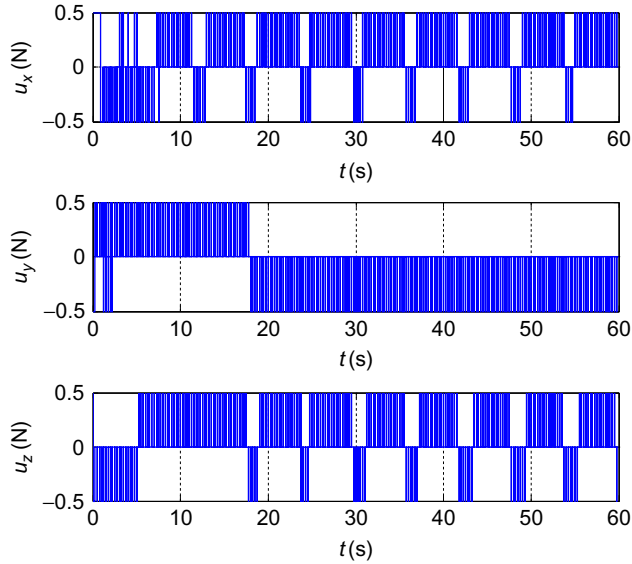

Fig. 8.10 Control force of the thruster.

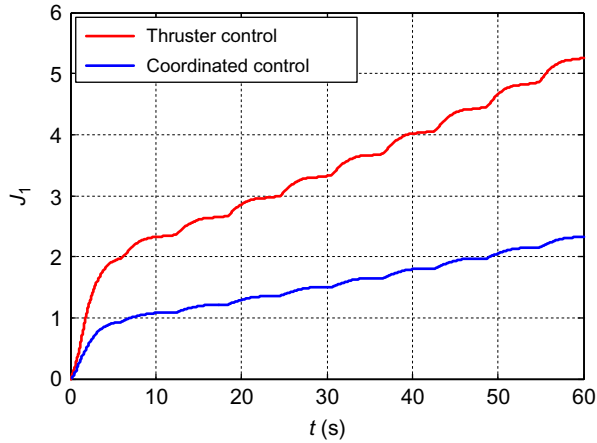

Fig. 8.11 Comparison of orbit control fuel consumption.

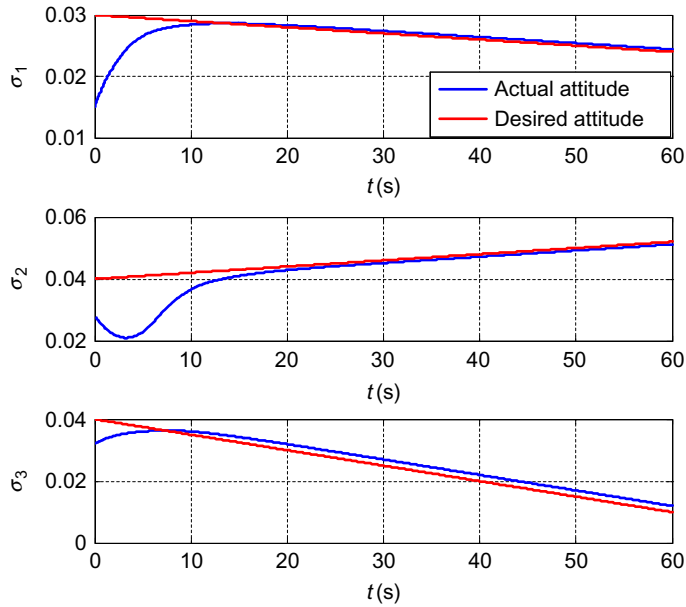

Fig. 8.12 MRP attitude tracking result of the TSR.

is shown in Fig. 8.16. The position of the mobile tether attachment point is located at the boundary of the feasible region of the back plane during the initial stage. The reason why this phenomenon occurs is that great control torques are required to stabilize the initial attitude tracking errors. The

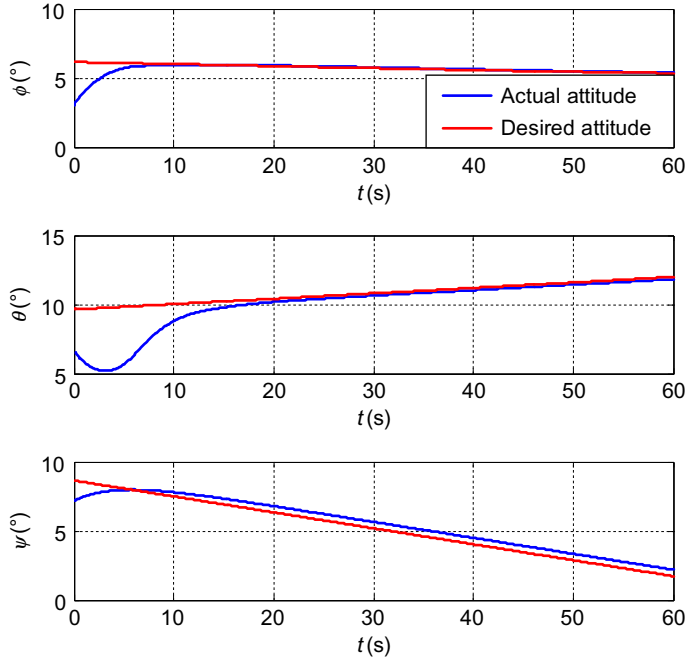

Fig. 8.13 Euler attitude tracking result of the gripper.

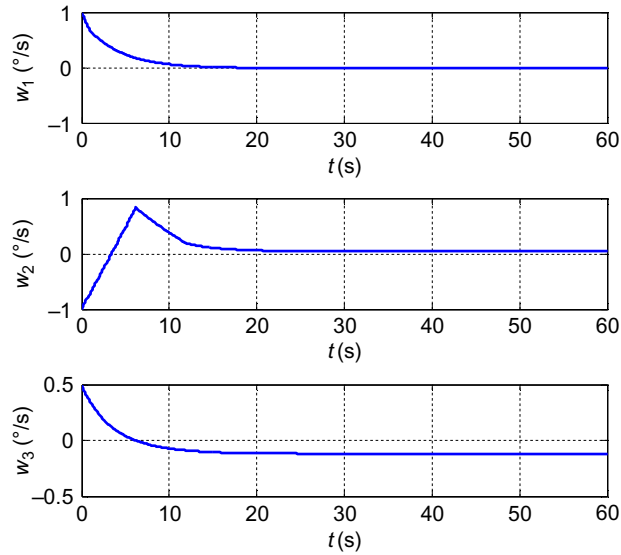

Fig. 8.14 Angular velocity of the TSR.

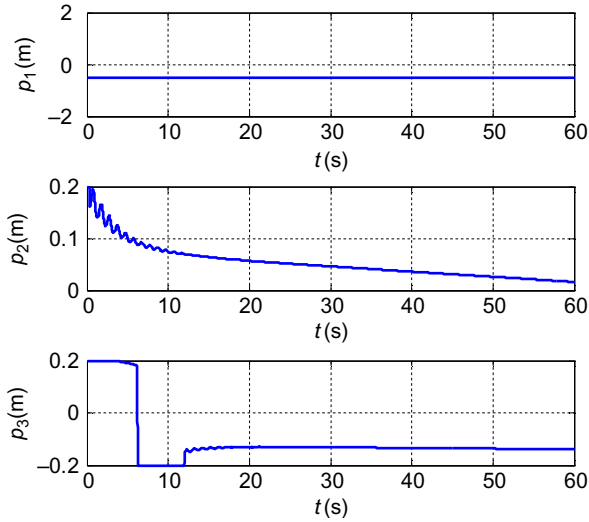

Fig. 8.15 Position of the mobile tether attachment point.

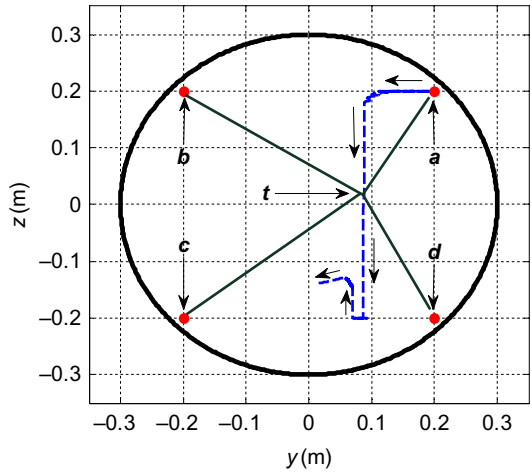

Fig. 8.16 Trajectory of the mobile tether attachment point.

position of the mobile tether attachment point changes slowly as the desired attitude changes in the final stage of the attitude control. Fig. 8.17 shows the length variation of these four tethers.

Fig. 8.18 shows the desired control torques, which are obtained by the coordinated controller Eq. (8.23), and the control torques generated by the thruster and the coordinated control mechanism are respectively illustrated

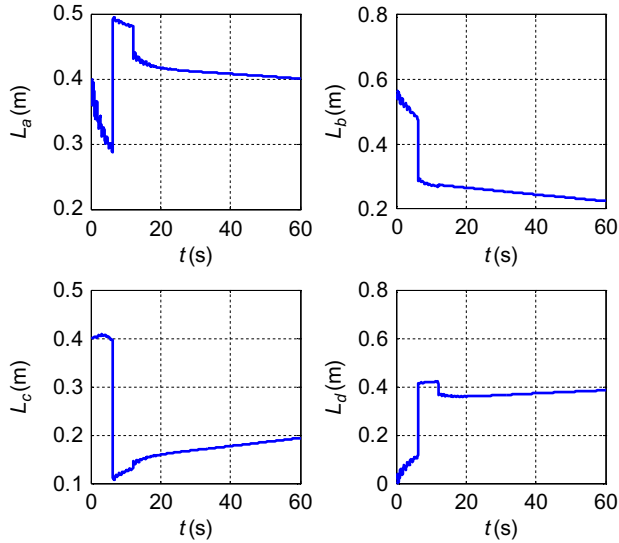

Fig. 8.17 Lengths of the tethers.

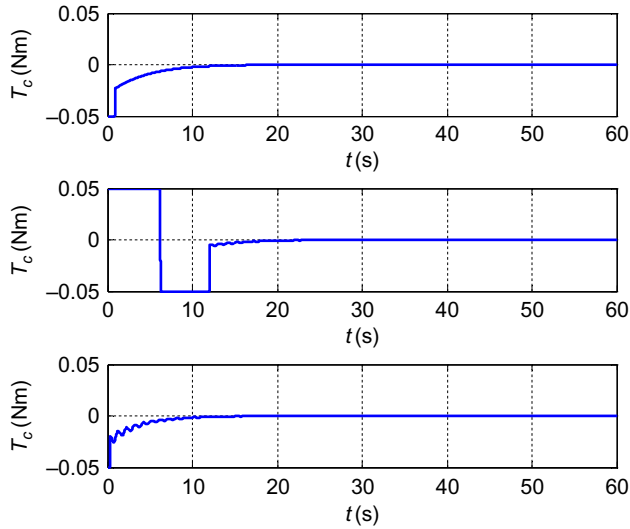

Fig. 8.18 Desired control torque of the gripper.

in Figs. 8.19 and 8.20. The pitch and yaw control torques of the latter are not consistency with these of the desired control torques. The region where the mobile tether attachment point moves is constrained. Therefore the control torques generated by the mechanism are also bounded. Besides, the disturbing torque caused by the coordinated control mechanism, which is less than

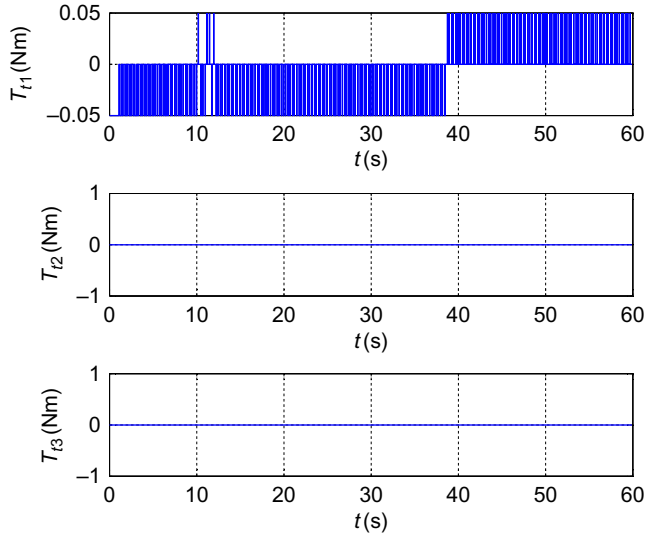

Fig. 8.19 Control torque of the thruster.

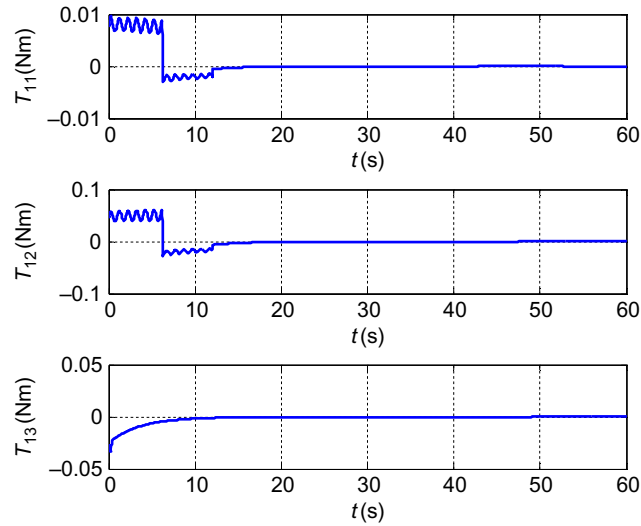

Fig. 8.20 Control torque of the tether.

0.01 Nm in the roll motion, is compensated by the control torques of the thrusters, as indicated in Figs. 8.12 and 8.13.

The fuel consumption function of attitude control is defined as follows:

$$\boldsymbol{J}_2 = \int_{t_0}^{t_f} \boldsymbol{T}_t^T \boldsymbol{T}_t dt \tag{8.50}$$

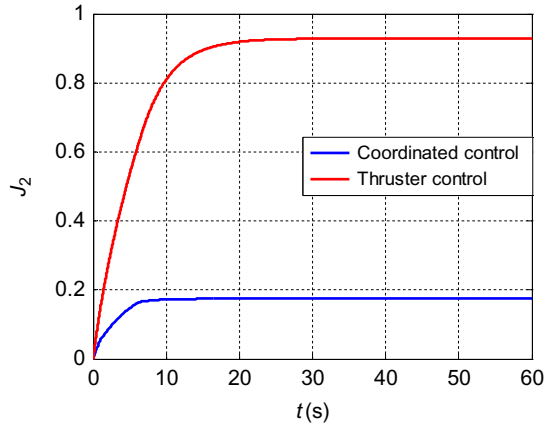

Fig. 8.21 Comparison of attitude control fuel consumption.

Fig. 8.21 compares the fuel consumption of the coordinated control and the traditional thruster control. The fuel consumption of the attitude coordinated control is the only fuel consumption of the control in the roll motion. The final fuel consumption of the coordinated control is 0.176, while that of the thruster control is 0.928, almost five times that of the former. This result demonstrates that the utilization of the coordinated control mechanism can reduce fuel consumption of the attitude control.

REFERENCES

[1] S. Pradeep, A new tension control law for deployment of tethered satellites, Mech. Res. Commun. 24 (3) (1997) 247–254.
[2] Y. Nakamura, S. Fumiki, N. Shinichi, Guidance and control of tethered retriever with collaborative tension-thruster control for future on-orbit service missions, in: Proceedings of the 8th International Symposium on Artificial Intelligence, Robotics and Automation in Space (i-SAIRAS 2005), 2005.
[3] K.K. Mankala, K.A. Sunil, A boundary controller based on linear infinite dimensional system for station keeping of a tethered satellite system, in: IEEE American Control Conference, 2006, 2006.
[4] V.J. Modi, S. Pradhan, A.K. Misra, Off-set control of the tethered systems using a graph theoretic approach, Acta Astronaut. 35 (6) (1995) 373–384.
[5] A. Djebli, M. Pascal, L. El Bakkali, Laws of deployment/retrieval in tether connected satellites systems, Acta Astronaut. 45 (2) (1999) 61–73.
[6] G. Liu, et al., Nonlinear dynamics and station-keeping control of a rotating tethered satellite system in halo orbits, Chin. J. Aeronaut. 26 (5) (2013) 1227–1237.
[7] M. Nohmi, T. Yamamoto, T. Youhei, Microgravity experiment for attitude control of a tethered body by arm link motion, in: IEEE International Conference on Mechatronics and Automation, 2007 (ICMA 2007), 2007.

[8] M. Nohmi, Attitude control of a tethered space robot by link motion under microgravity, in: Proceedings of the 2004 IEEE International Conference on Control Applications, 2004, vol. 1, IEEE, 2004.
[9] M. Nohmi, Mission design of a tethered robot satellite "STARS" for orbital experiment, in: 2009 IEEE Control Applications (CCA) & Intelligent Control (ISIC), IEEE, 2009.
[10] K.D. Kumar, B. Tan, Nonlinear optimal control of tethered satellite systems using tether offset in the presence of tether failure, Acta Astronaut. 66 (9) (2010) 1434–1448.
[11] K.D. Kumar, K. Kumar, Satellite pitch and roll attitude maneuvers through very short tethers, Acta Astronaut. 44 (5) (1999) 257–265.
[12] P.B. Beda, On requirements for attitude dynamics and stability control for tethered satellite systems, JSME Int. J., Ser. C 43 (3) (2000) 678–683.
[13] O. Mori, M. Saburo, Formation and attitude control for rotational tethered satellite clusters, J. Spacecr. Rocket. 44 (1) (2007) 211–220.
[14] I. Chang, P. Sang-Young, C. Kyu-Hong, Nonlinear attitude control of a tether-connected multi-satellite in three-dimensional space, IEEE Trans. Aerosp. Electron. Syst. 46 (4) (2010) 1950–1968.
[15] C. Menon, C. Bombardelli, Self-stabilising attitude control for spinning tethered formations, Acta Astronaut. 60 (10) (2007) 828–833.
[16] S. Bergamaschi, F. Bonon, Coupling of tether lateral vibration and subsatellite attitude motion, J. Guid. Control. Dyn. 15 (5) (1992) 1284–1286.
[17] Godard, J.L. Crassidis, F.L. Markley, Sliding mode control using modified rodrigues parameters, J. Guid. Control. Dyn. 19 (6) (1996) 1381–1383.
[18] G.Q. Xing, S.A. Parvez, Nonlinear attitude state tracking control for spacecraft, J. Guid. Control. Dyn. 24 (3) (2001) 624–626.
[19] P.E. Gill, W. Murray, M.A. Saunders, SNOPT: an SQP algorithm for large-scale constrained optimization, SIAM J. Optim. 12 (4) (2002) 979–1006.
[20] C. Guan, S. Zhu, Adaptive time-varying sliding mode control for hydraulic servo system, in: 8th International Conference on Control, Automation, Robotics and Vision, 2004 (ICARCV 2004), vol. 3, IEEE, 2004.